Freshwater pulse experiments

The experiments in Fig. 4a simulate deglacial meltwater discharge to the Atlantic Ocean between 20°N and 50°N. Experiment LGM_CTRL_H500 and LGM_SH_H500 display the model response to a 500-year freshwater-pulse of 0.15 Sv. The starting point of experiment LGM_SH_Hperm, representing the THC 'off-mode', results from a permanent freshwater flow of 0.15 Sv to the glacial equilibrium state. The freshwater flow persists during this experiment. In LGM_SH_H500 and LGM_SH_Hperm, Southern Hemisphere warming is executed as in LGM_100, while the glacial background conditions in experiment LGM_CTRL_H500 remain unaltered.

Stability analysis

We apply a slowly varying freshwater anomaly with a rate of 5×10^{-5} Sv yr^{-1} (1×10^{-6} Sv yr^{-1} at the transition of the hysteresis curve that starts from LGM_100) uniformly between 20° N and 50° N to the Atlantic Ocean. Integration starts at the upper branches with zero freshwater forcing, which is then increased up to 0.2 Sv and 0.32 Sv for LGM_CTRL and LGM_100, respectively. The integration proceeds on the lower branch with freshwater input decreasing until −0.12 Sv. Then the freshwater increases again to close the loops. Owing to the slowly varying nature of the surface forcing the model is in quasi-equilibrium during the integration.

Received 21 November 2002; accepted 23 June 2003; doi:10.1038/nature01855.

1. Sowers, T. & Bender, M. Climate records covering the last deglaciation. *Science* **269,** 210–214 (1995).
2. Petit, R. *et al.* Climate and atmospheric history of the past 420,000 years from the Vostok ice core, Antarctica. *Nature* **399,** 429–436 (1999).
3. Marshall, J. S. & Clarke, G. K. C. Modelling North American freshwater runoff through the last glacial cycle. *Quat. Res.* **52,** 300–315 (1999).
4. Stocker, T. F. & Wright, D. G. Rapid transitions of the ocean's deep circulation induced by changes in surface water fluxes. *Nature* **351,** 729–732 (1991).
5. Maier-Reimer, E., Mikolajewicz, U. & Hasselmann, K. Mean circulation of the Hamburg LSG OGCM and its sensitivity to the thermohaline surface forcing. *J. Phys. Oceanogr.* **23,** 731–757 (1993).
6. Sarnthein, M. *et al.* Changes in east Atlantic deepwater circulation over the last 30,000 years: Eight time slice reconstructions. *Paleoceanography* **9,** 209–267 (1994).
7. Prange, M., Romanova, V. & Lohmann, G. The glacial thermohaline circulation: Stable or unstable? *Geophys. Res. Lett.* **29,** 10.1029/2002GL015337 (2002).
8. Shemesh, A. *et al.* Sequence of events during the last deglaciation in Southern Ocean sediments and Antarctic ice cores. *Paleoceanography* **17,** 101029/2000PA000599 (2002).
9. Gordon, A. L., Weiss, R. F., Smethie, W. M. Jr & Warner, M. J. Thermocline and intermediate water communication between the South Atlantic and Indian Oceans. *J. Geophys. Res.* **97,** 7223–7240 (1992).
10. Broecker, W. S. The great ocean conveyor. *Oceanography* **4,** 79–89 (1991).
11. Shin, S. I., Otto-Bliesner, B., Brady, E. C., Kutzbach, J. E. & Harrison, S. P. A simulation of the last glacial maximum climate using the NCAR-CCSM. *Clim. Dyn.* **20,** 127–151 (2003).
12. Ganopolski, A. & Rahmstorf, S. Rapid changes of glacial climate simulated in a coupled climate model. *Nature* **409,** 153–158 (2001).
13. Macdonald, A. M. & Wunsch, C. An estimate of global ocean circulation and heat fluxes. *Nature* **382,** 436–439 (1996).
14. Weijer, W., De Ruijter, W. P. M., Sterl, A. & Drijfhout, S. S. Response of the Atlantic overturning circulation to South Atlantic sources of buoyancy. *Glob. Planet. Change* **34,** 293–311 (2002).
15. Stommel, H. Thermohaline convection with two stable regimes of flow. *Tellus* **13,** 224–230 (1961).
16. Stocker, T. F. in *Continuum Mechanics and Applications in Geophysics and the Environment* (eds Straugham, B., Greeve, R., Ehrentraut, H. & Wang, Y.) 337–367 (Springer, New York, 2001).
17. Rühlemann, C., Mulitza, S., Müller, P. J., Wefer, G. & Zahn, R. Warming of the tropical Atlantic Ocean and slowdown of thermohaline circulation during the last deglaciation. *Nature* **402,** 511–514 (1999).
18. Bard, E., Rostek, F., Turon, J. L. & Gendreau, S. Hydrological impact of Heinrich events in the subtropical northeast Atlantic. *Science* **289,** 1321–1324 (2000).
19. Sachs, J. P., Anderson, R. F. & Lehman, S. J. Glacial surface temperatures of the southeast Atlantic Ocean. *Science* **293,** 2077–2079 (2001).
20. Crowley, T. J. North Atlantic Deep Water cools the Southern Hemisphere. *Paleoceanography* **7,** 489–497 (1992).
21. Stephens, B. B. & Keeling, R. F. The influence of Antarctic sea ice on glacial–interglacial CO_2 variations. *Nature* **404,** 171–174 (2000).
22. Toggweiler, J. R. Variation of atmospheric CO_2 by ventilation of the ocean's deepest water. *Paleoceanography* **14,** 571–588 (1999).
23. Lohmann, G. & Schulz, M. Reconciling Bølling warmth with peak deglacial meltwater discharge. *Paleoceanography* **15,** 537–540 (2000).
24. Schott, W. Die Foraminiferen in dem äquatorialen Teil des Atlantischen Ozeans. *Deut. Atl. Exped. Meteor* 1925–1927 **3,** 43–134 (1935).
25. Berger, W. H. & Wefer, G. in *The South Atlantic: Present and Past Circulation* (eds Wefer, G., Berger, W. H., Siedler, G. & Webb, D. J.) 363–410 (Springer, Heidelberg, 1996).
26. Kim, S. J., Crowley, T. J. & Stössel, A. Local orbital forcing of Antarctic climate change during the last interglacial. *Science* **280,** 728–730 (1998).
27. Koutavas, A., Lynch-Stieglitz, J., Marchitto, T. M. Jr & Sachs, J. P. El Niño-like pattern in ice age tropical Pacific sea surface temperature. *Science* **297,** 226–230 (2002).
28. Schouten, M. W., De Ruijter, P. M. & van Leeuwen, P. J. Upstream control of Agulhas Ring shedding. *J. Geophys. Res.* **107** 101029/2001JC000804 (2002).
29. Prange, M., Lohmann, G. & Paul, A. Influence of vertical mixing on the thermohaline hysteresis: Analyses of an OGCM. *J. Phys. Oceanogr.* **33,** 1707–1721 (2003).
30. Lohmann, G. & Lorenz, S. The hydrological cycle under paleoclimatic boundary conditions as derived from AGCM simulations. *J. Geophys. Res.* **105,** 17417–17436 (2000).

Supplementary Information accompanies the paper on **www.nature.com/nature**.

Acknowledgements We thank H. Jansen, S. Mulitza and M. Prange for suggestions. L. Könnecke, S. Schubert, M. Butzin and S. Blessing are acknowledged for their technical support. This work was supported by BMBF through the DEKLIM project 'climate transitions'.

Competing interests statement The authors declare that they have no competing financial interests.

Correspondence and requests for materials should be addressed to G.K. (gregor.knorr@dkrz.de).

Possible thermal and chemical stabilization of body-centred-cubic iron in the Earth's core

Lidunka Vočadlo[1], Dario Alfè[1,2], M. J. Gillan[2], I. G. Wood[1], J. P. Brodholt[1] & G. David Price[1]

[1]*Research School of Earth Sciences, Birkbeck College and University College London, and*
[2]*Department of Physics and Astronomy, University College London, Gower Street, London WC1E 6BT, UK*

The nature of the stable phase of iron in the Earth's solid inner core is still highly controversial. Laboratory experiments[1] suggest the possibility of an uncharacterized phase transformation in iron at core conditions and seismological observations[2–4] have indicated the possible presence of complex, inner-core layering. Theoretical studies[5,6] currently suggest that the hexagonal close packed (h.c.p.) phase of iron is stable at core pressures and that the body centred cubic (b.c.c.) phase of iron becomes elastically unstable at high pressure. In other h.c.p. metals, however, a high-pressure b.c.c. form has been found to become stabilized at high temperature. We report here a quantum mechanical study of b.c.c.-iron able to model its behaviour at core temperatures as well as pressures, using *ab initio* molecular dynamics free-energy calculations. We find that b.c.c.-iron indeed becomes entropically stabilized at core temperatures, but in its pure state h.c.p.-iron still remains thermodynamically more favourable. The inner core, however, is not pure iron, and our calculations indicate that the b.c.c. phase will be stabilized with respect to the h.c.p. phase by sulphur or silicon impurities in the core. Consequently, a b.c.c.-structured alloy may be a strong candidate for explaining the observed seismic complexity of the inner core[2–4].

Seismic measurements show that the Earth's solid inner core is complex. The detailed interpretations of these data differ, but all workers[2–4] conclude that the inner core exhibits a significant degree of layering, which may either reflect the changing history of core crystallization, or the occurrence of an unidentified change in the core-forming phase. It is currently generally accepted that the core consists predominantly of Fe, and conventional interpretations of the elastic anisotropy of the inner core have been based on the idea of a partial alignment of crystals of h.c.p.-Fe[5]. Recently, however this interpretation has been challenged[3], as has the assumption that h.c.p.-Fe is the thermodynamically stable polymorph of Fe at the high temperatures found in the inner core[1]. The low pressure (P)–temperature (T) phase diagram of Fe is not controversial, with b.c.c.-Fe stable at ambient conditions, h.c.p.-Fe stable above about 15 GPa at low temperatures and the face-centred-cubic (f.c.c.) structure being stable above about 1,300 K at low pressures. High-P/T diamond-anvil-cell experiments[7] suggest a new phase above ~40 GPa and ~1,000 K, but the structure of this phase is still unresolved. In addition, a solid–solid phase transition at around

~200 GPa and ~4,000 K has been inferred from shock data[1].

In spite of the arguments in favour of h.c.p.-Fe, it has been proposed by a number of workers that b.c.c.-Fe might be the stable high-P/T phase[8,9]. A strong argument in favour of the stability of b.c.c.-Fe under these conditions is that a number of transition metals are known to transform from close-packed structures to the b.c.c. structure at temperatures just below their melting curve[10,11]. For Fe, the argument in favour of b.c.c. is further strengthened by *ab initio* calculations showing the existence of an appreciable magnetic moment in b.c.c.-Fe at Earth's core pressures[12], which implies an additional magnetic entropy stabilization at high temperatures. However, for a long time it appeared that theoretical calculations had ruled out the b.c.c. structure as a candidate for the stable phase of Fe in the core. This was for three reasons: (1) *ab initio* calculations have shown that the structure becomes elastically unstable at pressures above 150 GPa[12,13]; (2) *ab initio* calculations also reveal a high-pressure vibrational instability away from the zone centre[14]; (3) calculations show that the enthalpy of the perfect b.c.c. structure is considerably higher than that of the h.c.p. phase[6,12–14]. However, these arguments are not conclusive because they are based on athermal or lattice dynamical[6,12–14] *ab initio* calculations, which, because of the dynamical instability of b.c.c.-Fe, cannot be used to determine entropic effects at high pressures. In the past, computing limitations prevented a more sophisticated analysis, but recent methodological developments mean that it is now possible accurately to address these thermal effects. Thus, to resolve the controversy over the effect of temperature on the stability of b.c.c.-Fe, we report here *ab initio* molecular dynamics (AIMD) calculations on b.c.c.-Fe to simulate directly its behaviour at the high temperatures relevant to the Earth's inner core.

It is well established that *ab initio* calculations give an accurate description of all the key properties of Fe[12–15]. The calculations presented here are based on density functional theory (DFT)[16] within the generalized gradient approximation (GGA)[17]. They were performed using the VASP code[18], using the projected-augmented wave (PAW) method[19] to calculate the total energy of the system. The PAW method is closely related to the ultrasoft pseudopotential method and has been shown to give results that agree accurately with all-electron methods[20,21]. In AIMD, the ions are treated as classical particles and, for each set of atomic positions, the electronic energy and forces on the ions are calculated within the framework of DFT, which includes the thermal excitations of the electrons.

The elastic and vibrational instabilities of high-pressure b.c.c.-Fe have been studied before[12–14], but because of their key role in this work, we present in Fig. 1 our own results for the phonon dispersion relations as a function of pressure. It can be seen that the onset of the instability of b.c.c.-Fe at high pressure occurs below ~180 GPa where one of the branches in the X [110] direction becomes unstable at the zone centre (associated with the elastic constant $c' = (c_{11} - c_{12})/2$ becoming negative). This instability is associated with the b.c.c. → f.c.c. transition[13]. However, there is also a second instability occurring below 260 GPa, along the [111] direction (Γ to L); the pattern of the displacement involved in this instability concerns the relative motion of planes of atoms in the [111] direction of the cubic cell. This pattern of displacement is directly involved in the b.c.c. → ω transition, a transition which is known to readily occur in other transition metals[10,11,22].

In order to establish whether the b.c.c. phase at high pressure is entropically stabilized by temperature, we performed AIMD at 6,000 K (approximate core temperatures[23,24]) for a chosen volume of 7.2 Å^3 per atom (approximate core density) and compared the results with those from simulations performed at lower temperatures. The stability of the b.c.c. structure at high temperatures was assessed in four separate ways: (1) the anisotropic stresses were analysed for evidence of elastic stability, (2) the atomic positions with respect to those in a perfect b.c.c. structure were analysed for evidence of vibrational stability, (3) the structure factors were calculated to help identify the phases present, (4) the relative free energy with respect to the h.c.p. structure was calculated in order to

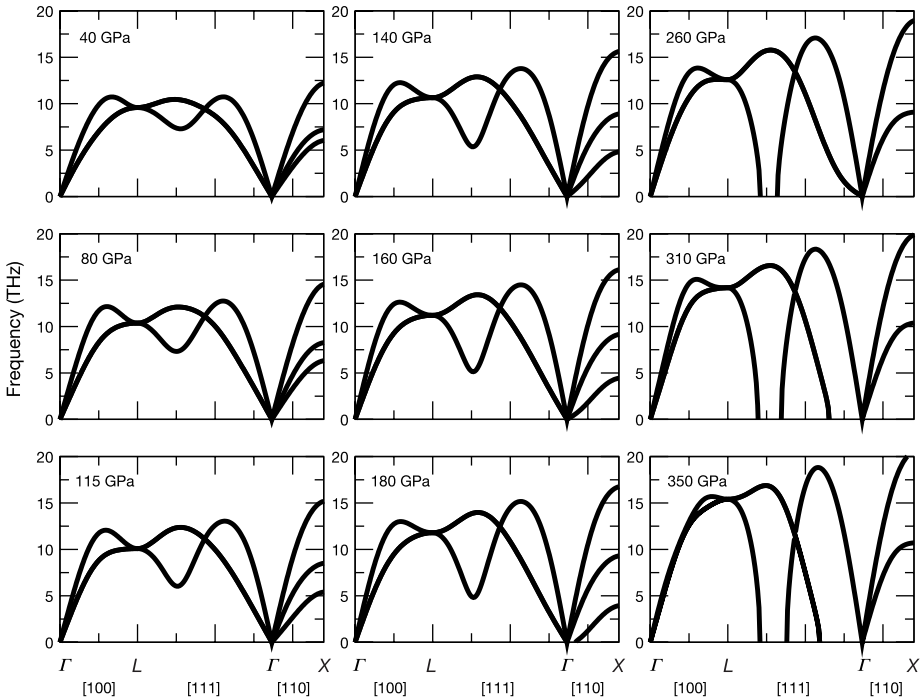

Figure 1 The calculated phonon dispersion curves for b.c.c.-Fe at nine different volumes (corresponding to ~40–350 GPa). The softening in the [110] direction at ~180 GPa indicates the onset of the b.c.c. → f.c.c. transition, and that in the [111] direction above ~260 GPa corresponds to the b.c.c. → ω transition. For these calculations, we used a 64-atom (4 × 4 × 4) cubic supercell with a 3 × 3 × 3 **k**-point sampling grid and the small-displacement method to obtain the vibrational frequencies, the methodology of which has been described elsewhere[21].

determine its thermodynamic stability at core conditions. The graph shown in the upper left corner of Fig. 2 gives the six components of the stress tensor of the cubic b.c.c. cell at 6,000 K as a function of simulation time; it can be seen that the supercell experiences hydrostatic stresses throughout the simulation, suggesting that the cell is stable. It is clear that when the temperature is considerably reduced (to below 3,000 K), the cell is no longer under hydrostatic stress, indicating that the b.c.c.-Fe structure is no longer elastically stable.

To identify whether the atoms in our simulation cell have moved away from the perfect b.c.c. structure, we can look at the positions of the atoms throughout the simulation relative to b.c.c. lattice sites. A convenient method for analysing the evolution of the atomic positions over the length of the simulation is to use the position correlation function, $p(t)$, which not only tells us where the atoms are, but also may indicate the existence of an imminent phase transition. The graph in the lower left corner of Fig. 2 shows $p(t)$ at 6,000 K; it is clear that $p(t) \rightarrow 0$ as $t \rightarrow \infty$, indicating that the atomic positions in the simulation cell are, on average, those of a perfect b.c.c. structure. We can therefore conclude that, at 6,000 K and a volume of 7.2 Å^3 per atom (approximate core pressures and temperatures), the b.c.c. structure is vibrationally stable. However, as the system is cooled, it can readily be seen that the atoms deviate significantly and permanently away from a b.c.c. structure (that is, $p(t) \neq 0$ as $t \rightarrow \infty$) below 3,000 K. In fact, analysis of the structure factors (not presented) show that the b.c.c. phase undergoes a transition to the ω phase.

Having established that the b.c.c. phase under pressure is elastically and vibrationally stable at high temperatures, we need to calculate its free energy at core conditions to determine its thermodynamic stability with respect to h.c.p. We use the method of thermodynamic integration, which allows us to calculate the difference in free energy, $F - F_0$, between our *ab initio* b.c.c. system and a reference system whose potential energies are U and U_0 respectively. Recently[21,23–25] we have successfully used this method to calculate *ab initio* the melting behaviour of Al at pressure, and the properties of liquid and h.c.p.-Fe. An important point to note is that these calculations were performed without spin polarization. As mentioned earlier, it is well known that the b.c.c. phase has a significant magnetic moment at core pressures[12], which, if maintained at high temperature, would contribute to the free energy through the disordering of the orientations of the spins. However, at high temperatures, the magnetic moment will be destroyed by thermal excitation of the electrons. We performed calculations on the b.c.c. structure at inner core pressures as a function of electronic temperature (2,000–6,000 K). Our results show that, as expected, the magnetic moment decreases with temperature, and disappears altogether well before core temperatures are reached; there is, therefore, no contribution to the free energy of b.c.c.-Fe from magnetic entropy.

Table 1 shows our calculated Helmholtz free energies for the b.c.c. and h.c.p. phases over a range of volumes and temperatures along (and below) our previously determined melting curve of h.c.p.-Fe[23–24]. It is clear that in all cases $F_{\text{b.c.c.}} > F_{\text{h.c.p.}}$. However, the differences in free energies are small (33–58 meV per atom along the melting temperature curve, T_m). The Earth's inner core, however, is

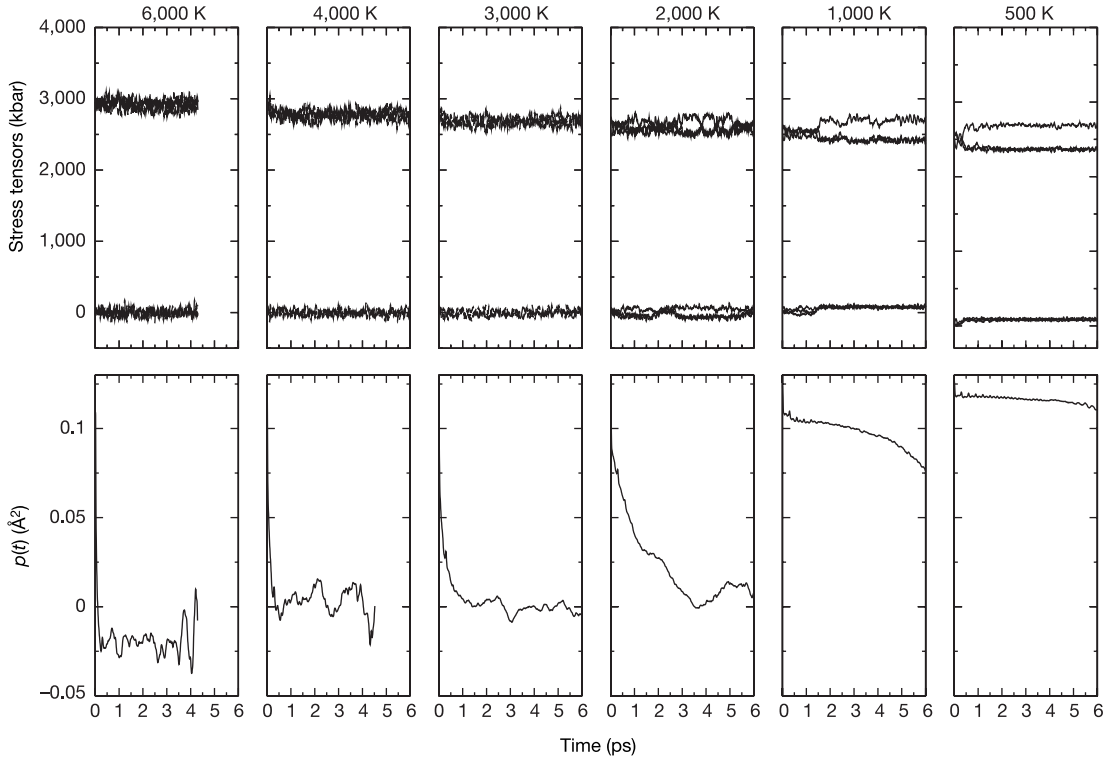

Figure 2 The calculated stress tensors as a function of simulation time (upper row) and position correlation functions (lower row) for a 64-atom cubic supercell at different temperatures. The structure deviates away from the b.c.c. phase below 3,000 K. We performed these high-temperature calculations on two supercells to ensure that any transition observed is not influenced by the size and shape of the simulation cell. We used both the 64-atom cubic supercell and a hexagonal supercell ($3 \times 3 \times 5$) of 135 atoms, since this latter setting provides us with a simulation cell which readily allows us to have within it an integral number of unit cells of both the b.c.c. and ω phases. The calculations were run initially at 6,000 K and then at successively lower temperatures, using a stable equilibrated high-temperature b.c.c. configuration as the starting configuration in each case. The position correlation function for a chosen atom, i, is given by $p(t) = \langle(\mathbf{r}_i(t+t_0) - \mathbf{R}_i^0)\cdot(\mathbf{r}_i(t_0) - \mathbf{R}_i^0)\rangle$, where $\mathbf{r}_i$ is the time-varying position of the atom and $\mathbf{R}_i^0$ is the position of that atom's lattice site in the perfect b.c.c. structure. The angular brackets denote the thermal average, which in practice is evaluated as an average over time origins, t_0, and atoms i. For long times t, vibrational displacements become uncorrelated, so that $p(t) = \langle(\mathbf{r}_i(t+t_0) - \mathbf{R}_i^0)\rangle\cdot\langle(\mathbf{r}_i(t_0) - \mathbf{R}_i^0)\rangle \rightarrow \langle\mathbf{r}_i - \mathbf{R}_i^0\rangle^2$, and if all atoms vibrate about b.c.c. lattice sites, $\langle\mathbf{r}_i - \mathbf{R}_i^0\rangle = 0$, so that $p(t) \rightarrow 0$ as $t \rightarrow \infty$.

Table 1 **Calculated Helmholtz free energy of the b.c.c. and h.c.p. phases of Fe**

Volume (Å^3)	Temperature (K)	$F_{b.c.c.}$ (eV)	$F_{h.c.p.}$ (eV)	$\Delta F_{b.c.c.-h.c.p.}$ (meV)
9.0	3,500	−10.063	−10.109	46
8.5	3,500	− 9.738	− 9.796	58
7.8	5,000	−10.512	−10.562	50
7.2	6,000	−10.633	−10.668	35
6.9	6,500	−10.545	−10.582	37
6.7	6,700	−10.288	−10.321	33
*7.2	3,000	− 7.757	− 7.932	175

Shown is the *ab initio* Helmholtz free energy per atom of the b.c.c. and h.c.p. phases of Fe, $F_{b.c.c.}$ and $F_{h.c.p.}$, at state points along (*and below) the calculated melting curve[23]. In this work, the reference system is a simple inverse power potential which takes the form $U = 4\varepsilon(\Gamma/r)^\alpha$ where $\varepsilon = 1$ eV, $\Gamma = 1.77$ Å, $\alpha = 5.86$. We have previously shown that this reference potential, based on only a repulsive term, describes the *ab initio* system extremely well; the bonding term is almost independent of the atomic positions, depending only on the volume and temperature of the system[21,24]. We stress, however, that the final result is totally independent of the choice of reference system. We performed these calculations on a 64-atom supercell ($4 \times 4 \times 4$ primitive cells) with a $3 \times 3 \times 3$ **k**-point grid. Considerable effort was spent on convergence tests in **k**-point sampling to reduce the error in free energies to <10 meV per atom. Cell size effects have been extensively studied in our previous work on h.c.p.-Fe[21].

known not to be made of pure Fe, but is expected to be alloyed with between 5 to 10 mol.% of a lighter element. It is now reasonably well established that either separately or together S and Si are two of the most probable light elements alloyed with Fe in the core[26–29]. Additionally, recent experiments[30] have shown that at high pressures FeSi crystallizes with the CsCl-structure (that is, has identical atomic coordinates to b.c.c.-Fe), and at lower concentrations Si stabilizes b.c.c.-Fe under pressure and temperature conditions at which pure Fe is found with the h.c.p. structure[26]. We therefore investigated the energetic effect of the substitution of S and Si in b.c.c. and h.c.p.-Fe at representative core cell volumes (7.2 Å^3). We find that the enthalpies of the S and Si defects are respectively 1.4 and 1.2 eV per defect atom more stable in the b.c.c. structure than in the h.c.p. phase. Therefore, for example, a 5 mol.% concentration of Si in Fe, would stabilize the b.c.c. phase by 60 meV. Thus, in contrast with lower-pressure experiments[26], we conclude that the presence of S or Si as the light impurity element in the core, at appropriate concentrations, could favour the formation of a b.c.c.- rather than an h.c.p.-structured Fe alloy phase at temperatures just below T_m at inner core pressure.

In contrast to earlier work, we have shown that a b.c.c.-structured phase is entropically stabilized under inner core conditions, and is made more stable than the h.c.p.-phase by impurities in the inner core. This means that a b.c.c.-structured alloy is a strong candidate for explaining the recently observed[2–4] seismic complexity of the inner core. □

Received 21 August 2002; accepted 18 June 2003; doi:10.1038/nature01829.

1. Brown, M. J. The equation of state of iron to 450 GPa: Another high-pressure solid phase? *Geophys. Res. Lett.* **28,** 4339–4342 (2001).
2. Song, X. D. & Helmberger, D. V. Seismic evidence for an inner core transition zone. *Science* **282,** 924–927 (1998).
3. Beghein, C. & Trampert, J. Robust normal mode constraints on inner-core anisotropy from model space search. *Science* **299,** 552–555 (2003).
4. Ishii, M. & Dziewonski, A. M. The innermost inner core of the earth: Evidence for a change in anisotropic behavior at the radius of about 300 km. *Proc. Natl Acad. Sci. USA* **99,** 14026–14030 (2002).
5. Steinle-Neumann, G., Stixrude, L., Cohen, R. E. & Gülseren, O. Elasticity of iron at the temperature of the Earth's inner core. *Nature* **413,** 57–60 (2001).
6. Vočadlo, L., Brodholt, J., Alfè, D., Gillan, M. J. & Price, G. D. Ab initio free energy calculations on the polymorphs of iron at core conditions. *Phys. Earth Planet. Inter.* **117,** 123–137 (2000).
7. Shen, G. Y., Mao, H. K., Hemley, R. J., Duffy, T. S. & Rivers, M. L. Melting and crystal structure of iron at high pressures and temperatures. *Geophys. Res. Lett.* **25,** 373–376 (1998).
8. Ross, M., Young, D. A. & Grover, R. Theory of the iron phase diagram at Earth core conditions. *J. Geophys. Res.* **95,** 21713–21716 (1990).
9. Matsui, M. & Anderson, O. L. The case for a body-centred-cubic phase (α') for iron at inner core conditions. *Phys. Earth Planet Inter.* **103,** 55–62 (1997).
10. Petry, W. Dynamical precursors of martensitic transitions. *J. Phys. IV* **5,** C2-15–C2-28 (1995).
11. Trampenau, J. *et al.* Phonon dispersion of the bcc phase of group-IV metals. III. bcc hafnium. *Phys. Rev. B* **43,** 10963–10969 (1991).
12. Söderlind, P., Moriarty, J. A. & Willis, J. M. First-principles theory of iron up to Earth-core pressures: structural, vibrational and elastic properties. *Phys. Rev. B* **53,** 14063–14072 (1996).
13. Stixrude, L. & Cohen, R. E. Constraints on the crystalline structure of the inner core: mechanical instability of BCC iron at high pressures. *Geophys. Res. Lett.* **22,** 125–128 (1995).
14. Moriarty, J. A. in *High Pressure Science and Technology 1993* (eds Schmidt, S. C., Shaner, J. W., Samara, G. A. & Ross, M.) 233–236 (AIP Press, New York, 1994).
15. Mao, H. K. *et al.* Phonon density of states of iron up to 153 gigapascals. *Science* **292,** 914–916 (2001).
16. Hohenberg, P. & Kohn, W. Inhomogeneous electron gas. *Phys. Rev.* **136,** B864–B871 (1964).
17. Wang, Y. & Perdew, J. Correlation hole of the spin-polarized electron gas, with exact small-wave-vector and high-density scaling. *Phys. Rev. B* **44,** 13298–13307 (1991).
18. Kresse, G. & Furthmüller, J. Efficient iterative schemes for *ab initio* total-energy calculations using a plane-wave basis set. *Phys. Rev. B* **54,** 11169–11186 (1996).
19. Blöchl, P. E. Projector augmented-wave method. *Phys. Rev. B* **50,** 17953–17979 (1994).
20. Alfè, D., Kresse, G. & Gillan, M. J. Structure and dynamics of liquid iron under Earth's core conditions. *Phys. Rev. B* **61,** 132–142 (2000).
21. Alfè, D., Price, G. D. & Gillan, M. J. Thermodynamics of hexagonal-close-packed iron under Earth's core conditions. *Phys. Rev. B* **64,** 045123 (2001).
22. Grad, G. B. *et al.* Electronic structure and chemical bonding effects upon the bcc to Ω phase transition: *ab initio* study of Y, Zr, Nb and Mo. *Phys. Rev. B* **62,** 12743–12753 (2000).
23. Alfè, D., Gillan, M. J. & Price, G. D. The melting curve of iron at Earth's core pressures from *ab initio* calculations. *Nature* **401,** 462–464 (1999).
24. Alfè, D., Price, G. D. & Gillan, M. J. Iron under Earth's core conditions: liquid-state thermodynamics and high pressure melting curve from *ab initio* calculations. *Phys. Rev. B* **65,** 165118 (2002).
25. Vočadlo, L. & Alfè, D. *Ab initio* melting curve of the *fcc* phase of aluminium. *Phys. Rev. B* **65,** 214105 (2002).
26. Lin, J.-F., Heinz, D. L., Campbell, A. J., Devine, J. M. & Shen, G. Iron-silicon alloy in Earth's core? *Science* **295,** 313–315 (2002).
27. Alfè, D., Price, G. D. & Gillan, M. J. Composition and temperature of the Earth's core constrained by combining ab initio calculations and seismic data. *Earth Planet. Sci. Lett.* **195,** 91–98 (2002).
28. Alfè, D., Price, G. D. & Gillan, M. J. *Ab initio* chemical potentials of solid and liquid solutions and the chemistry of the Earth's core. *J. Chem. Phys.* **116,** 7127–7136 (2002).
29. Alfè, D., Gillan, M. J. & Price, G. D. Constraints on the composition of the Earth's core from *ab-initio* calculations. *Nature* **405,** 172–175 (2000).
30. Dobson, D. P., Vočadlo, L. & Wood, I. G. A new high-pressure phase of FeSi. *Am. Mineral.* **87,** 784–787 (2002).

Acknowledgements L.V. and D.A. thank the Royal Society for their continued support through the University Fellowship scheme. We also thank NERC for providing computing facilities via grants.

Competing interests statement The authors declare that they have no competing financial interests.

Correspondence and requests for materials should be addressed to L.V. (l.vocadlo@ucl.ac.uk).

Measuring fast neutrons in Hiroshima at distances relevant to atomic-bomb survivors

T. Straume[1,2], G. Rugel[3,4], A. A. Marchetti[2], W. Rühm[4], G. Korschinek[3], J. E. McAninch[2], K. Carroll[2], S. Egbert[5], T. Faestermann[3], K. Knie[3], R. Martinelli[2], A. Wallner[3,4] & C. Wallner[3]

[1]*University of Utah, 729 Arapeen Drive, Suite 2334, Salt Lake City, Utah 84108, USA*
[2]*Lawrence Livermore National Laboratory (LLNL), PO Box 808, Livermore, California 94550, USA*
[3]*Technische Universität München, D-85747 Garching, Germany*
[4]*Ludwig Maximilians Universität München, D-80336, München, Germany*
[5]*Science Applications International Corporation, 10260 Campus Point Drive, San Diego, California 92121, USA*

Data from the survivors of the atomic bombs serve as the major basis for risk calculations of radiation-induced cancer in humans[1]. A controversy has existed for almost two decades, however, concerning the possibility that neutron doses in Hiroshima may have been much larger than estimated. This controversy was based on measurements of radioisotopes activated by thermal neutrons that suggested much higher fluences at larger distances than expected[2–6]. For fast neutrons, which contributed almost all the neutron dose, clear measurement validation has so far proved impossible at the large distances (900 to 1,500 m) most relevant to survivor locations[6]. Here, the first